Highlights

- A wear prediction method of the piston/cylinder pair which can obtain the time-varying wear process of the piston/cylinder pair is established.
- The interaction between load-bearing and lubrication parameters and surface wear is taken into account.
- Both the experimental result and the simulation result show that the wear of two ends of the cylinder bore is relatively serious in the specific ranges of circumferential angle.
- The wear process can be divided into the steady wear stage and the severe wear stage according to the wear rate and the maximum wear depth.

Research on wear prediction of piston/cylinder pair in axial piston pumps

Fei Lyu[1], Junhui Zhang[1*], Guangming Sun[2], Bing Xu[1], Min Pan[3], Xiaochen Huang[1], Haogong Xu[1]

1 State Key Laboratory of Fluid Power and Mechatronic Systems, Zhejiang University, No.38 Zheda Road, Hangzhou, 310027, China

2 Linde Hydraulics (China) Co., Ltd., Weifang, 261000, China

3 Department of Mechanical Engineering, University of Bath, Bath BA2 7AY, Avon, UK

* Corresponding Author: Junhui Zhang. E-mail address: benzjh@zju.edu.cn

Abstract

The piston/cylinder pair is the critical lubricating interface of axial piston pumps. It suffers from excessive wear, especially under high output pressure. The performance degradation of the piston/cylinder pair is significant to be clarified. In this paper, a wear prediction method of the piston/cylinder pair is established by coupling the load-bearing and lubrication parameters calculation model and the wear calculation model. The models are validated through experiments. The experimental and simulated results show that the wear of two ends of the cylinder bore is severe in the specific ranges of circumferential angle. The time-varying wear process of the piston/cylinder pair can be obtained by using this method; therefore, the maintenance time can be predicted.

Keywords: piston/cylinder pair, wear prediction, load-bearing and lubrication parameters, axial piston pump

1. Introduction

Axial piston pumps are important power components in hydraulic fluid power systems, which are widely applied in aerospace, industrial and mobile machinery for its high-power density [1]. **Fig. 1** shows the general configuration of the axial piston pump which is comprised of a valve plate, a cylinder block, several pistons and slippers, a swash plate, and a shaft. Axial piston pump can be defined as a positive displacement pump, in which the hydraulic fluid is sucked and discharged through the change of the piston chamber volumes [2]. The piston is connected with the slipper which clings on the inclined swash-plate. When the pump operates, the cylinder block is driven by the shaft and rotates about the shaft. The pistons and the slippers rotate about the shaft with the cylinder block. Due to the slipper and the inclined swash plate, the pistons reciprocate within the cylinder bore, and the piston chamber volumes change. The friction pair between the piston and the cylinder bore is called piston/cylinder pair.

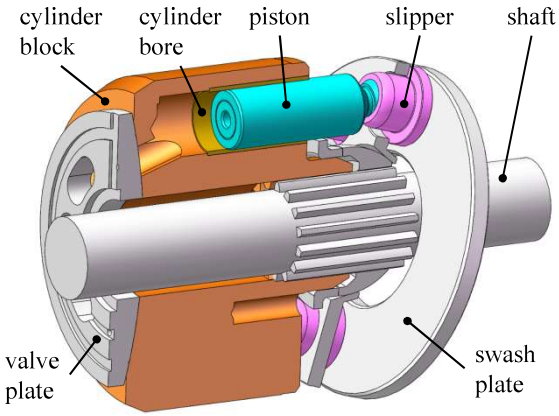

Fig. 1: General configuration of axial piston pump

It is urgent for piston pumps to be more compact and lightweight to meet the increasingly stringent requirements of different applications. One of the most effective methods to enhance the power/weight ratio is enhancing the working pressure. However, the force condition of the piston/cylinder pair is extremely severe under high working pressure, and the possibility of excessive wear significantly increases[3, 4]. As one of the critical friction pairs of axial piston pump, the excessive wear of the piston/cylinder pair could deteriorate the oil suction and discharging and lead to the failure of the pump. In order to react in due time and avoid unplanned machine breakdown, it is important to clarify the wear process of piston/cylinder pair. The oil film between the clearance of friction pairs of axial piston pump has a function of lubricating and sealing. The distribution characteristics of oil film, such as pressure and thickness, directly reflect the load-bearing and lubrication condition of the sliding surface, which determines whether the piston/cylinder pair is under dry friction, boundary friction or fluid friction [5]. Moreover, the surface micromorphology of piston/cylinder pair changes along with the wear process, which causes the oil film characteristics to change accordingly. Therefore, there is a strong interaction between the oil film characteristics and wear of the piston/cylinder pair.

Researchers are conducting the investigations on the oil film characteristics investigation of the axial piston pumps. Kolk [6] firstly obtained the pressure distribution of the oil film between the piston/cylinder pair by solving Reynold Equation, but the piston/cylinder pair was simplified to a sloping plain bearing with a load on the side edge which is quite different from the actual situation. More realistic force analysis was considered by Fang and Shirakashi [7], and they numerically calculated the thickness field of the oil film between the piston/cylinder pair. Furthermore, Ivantysynova, et al. [8-10] considered the non-isothermal flow conditions based on the energy equation, and a complete numerical simulation model of oil film characteristics calculation has been developed. There are several theoretical analysis platforms of friction pair oil film for axial piston pumps such as CASPAR [11], PUMA [12-15] and ViSPA [16], which are useful and valuable for the design and optimization of friction pairs of axial piston pump. However, it is noticed that the effect of wear on the oil film bearing surface is not considered in these theoretical models. Therefore, the capability of analysing the change of oil film characteristics with a long operating time is limited.

Many fundamental wear theories have been proposed [17-19] and are widely used in wear analysis of combustion engine, plain bearing, railway wheel-rail. Mayer and Ting [20] established a wear analysis model of the piston ring/cylinder liner system based on Archard wear model. Nautiyal [21] conducted experimental investigations to verify the simulated wear conditions between the piston ring and cylinder liner. For further calculation process, Bartel, et al. [22] introduced a computational model for calculating transient wear characteristics of plain bearings, and the modifications to the rough surfaces resulting from the running-in process are taken into consideration. Comparing with the piston ring/cylinder liner of the engine and the plain bearing, longer axial length of friction surface of the piston/cylinder pair could result in more complicated force condition of the piston. There is few research on the wear process of friction pairs in the field of the axial piston pump. Ma et al [23] presented an approach to analyze the wear behavior of swash plate/slipper pair considering the temperature, the outlet pressure and the rotational speed. But the wear process with an operating time cannot be clarified by using this method which neglects the distribution characteristics of oil film.

In this paper, a wear prediction method that considers the interaction between load-bearing and lubrication parameters and surface wear of piston/cylinder friction pair is proposed. Using this method, the time-varying wear profile of the entire cylinder bore can be achieved and analyzed. The accelerated lifetime investigation on an axial piston pump was conducted, and the wear profile of piston/cylinder pair was measured to determine the wear coefficient and verify the simulated results. The paper is outlined as follows: the simulation model is proposed and explained in detail in Section 2; Section 3 presents the establishment of the test rig and experimental results; Validation of the simulation models is conducted through real-time experiments. A comprehensive discussion is given in Section 4, followed by the conclusions in Section 5.

2. New Analytical Models

2.1. Dynamic analysis of piston/cylinder pair

The main external forces applied on the piston are shown in **Fig. 2**. The supporting force of the swash plate F_{SS} and the pressure force F_p enable the piston to reciprocate in the cylinder bore. F_{SSy} is the lateral component of F_{SS}. The friction force of slipper F_{FS} is generated by the sliding of slipper on the swash plate. The resultant force of F_{SSy} and F_{FS} is F_L. F_{FC} is the friction force between the cylinder and the piston, F_C is the centrifugal force of the piston, F_I is the inertia force of the piston. F_G is the gravity of the piston.

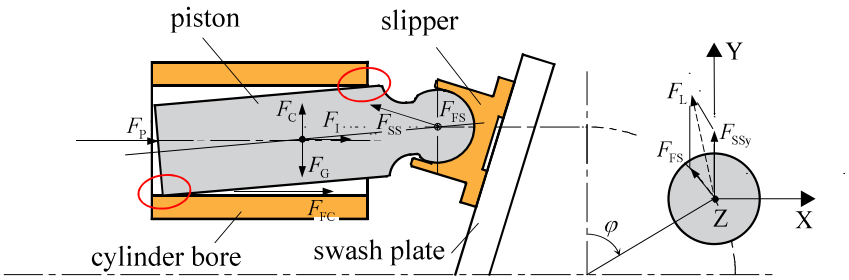

Fig. 2: External forces applied on the piston

The tiny clearance between the piston/cylinder pair and the large lateral force F_L cause the tilt of the piston in the cylinder bore. The squeezing effect of the oil film will be generated by the radial motion, and the dynamic pressure effect of wedge-shaped oil film will be generated with the motion of the piston. As indicated in the red cycle in **Fig. 2**, the solid contact pressure will be formed if the thickness of oil film at that position is very tiny. The reaction force which is in balance with the external forces is produced by the squeezing effect, the dynamic pressure effect and the solid contact pressure. The force and moment equilibrium equations of the piston are given as:

$$\begin{cases} F_X = F_{extX} + F_{oilX} + F_{conX} = 0 \\ F_Y = F_{extY} + F_{oilY} + F_{conY} = 0 \\ M_X = M_{extX} + M_{oilX} + M_{conX} = 0 \\ M_Y = M_{extY} + M_{oilY} + M_{conY} = 0 \end{cases} \tag{1}$$

where F_{extX}, F_{extY}, M_{extX} and M_{extY} are the external forces and moments, F_{oilX}, F_{oilY}, M_{oilX} and M_{oilY} are the reaction forces and moments generated by the hydrodynamic pressure of the oil film, F_{conX}, F_{conY}, M_{conX} and M_{conY} are the reaction forces and moments generated by the solid contact pressure of the piston and the cylinder bore, F_X, F_Y, M_X and M_Y are the resultant forces and moments in X and Y directions, respectively.

F_{oil} and F_{con} reflect the load-bearing condition of the piston/cylinder pair. Therefore, the hydrodynamic pressure of the oil film p and the solid contact pressure of the piston and cylinder bore p_s can be defined as the load-bearing parameters of the piston/cylinder pair. The oil film thickness is defined as the thickness of the lubricating film between the piston/cylinder pair. The load-bearing and lubrication parameters (LBLPs) of the piston/cylinder pair consist of the hydrodynamic pressure p, the solid contact pressure p_s and the oil film thickness h. LBLPs are scattered and different in the entire oil film field, and they need to be solved to determine the lubricating condition and wear process.

2.2. Calculation of LBLPs

A numerical model is created to calculate the distributive LBLPs of the piston/cylinder pair.

The oil film thickness between the piston/cylinder pair is related to the posture of the piston in the cylinder bore. When the surface wear occurs, the wear depth $w(l, \theta)$ must be considered to achieve

more accurate oil film thickness. **Fig. 3** shows the titling state of the piston in the cylinder bore exaggeratedly.

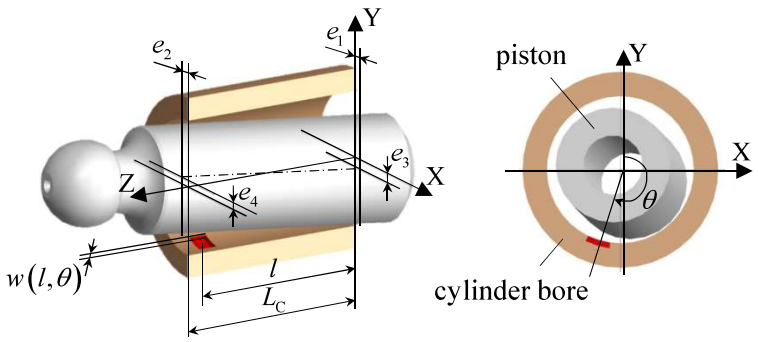

Fig. 3: Titling state of the piston

The posture of the piston can be represented by the eccentricities of two sections relative to the cylinder bore. The oil film thickness can be defined as the clearance between the piston and the cylinder bore in the radial direction, and it is given by:

$$h(l,\theta)=(D_C-D_P)/2+w(l,\theta)-\left[e_1-(e_1-e_2)l/L_C\right]\cos(\theta)-\left[e_3-(e_3-e_4)l/L_C\right]\sin(\theta) \tag{2}$$

where e_1 and e_2 are the eccentricities in the X direction of the two sections, respectively. e_3 and e_4 are the eccentricities in the Y direction of the two sections, respectively. L_C is the length of the cylinder bore, D_C is the diameter of the cylinder bore, and D_P is the diameter of the piston.

The elastic deformation could occur on the piston and the cylinder bore when their surfaces contact. There are rough peaks on the surface of piston and cylinder bore. Therefore, a minimum contact oil film thickness h_m can be determined by the surface roughness of the friction pair is set to estimate whether the contact occurs. The cross-section of the piston/cylinder pair in the case of critical contact is shown in **Fig. 4**(b). The definition of h_m [24]is shown as:

$$h_m = 3\sqrt{R_{qp}^{\ 2}+R_{qc}^{\ 2}} \tag{3}$$

where R_{qp} and R_{qc} are the root mean square (RMS) roughness of the piston and the cylinder bore respectively.

Both the piston and the cylinder bore are considered to be elastic. The elastic deformation occurs when the oil film thickness is thinner than h_m. The elastic deformation Δh is shown in **Fig. 4**(c) and can be calculated as using Eq. 4:

$$\Delta h=\begin{cases}0 & h(l,\theta)\ge h_m\\ h_m-h(l,\theta) & h(l,\theta)<h_m\end{cases} \tag{4}$$

It can be seen that Δh is the result of the elastic deformation of the piston and that of the cylinder bore. The solid contact pressure p_s generated by the elastic deformation of the piston and the cylinder bore can be solved using Eq. 5[25]:

$$\Delta h=p_s D_p/E_p+p_s H_c/E_c \tag{5}$$

where E_p and E_c are the elasticity modulus of the piston and the cylinder bore respectively, D_p is the diameter of the piston, H_c is the thickness of the cylinder block in the radial direction.

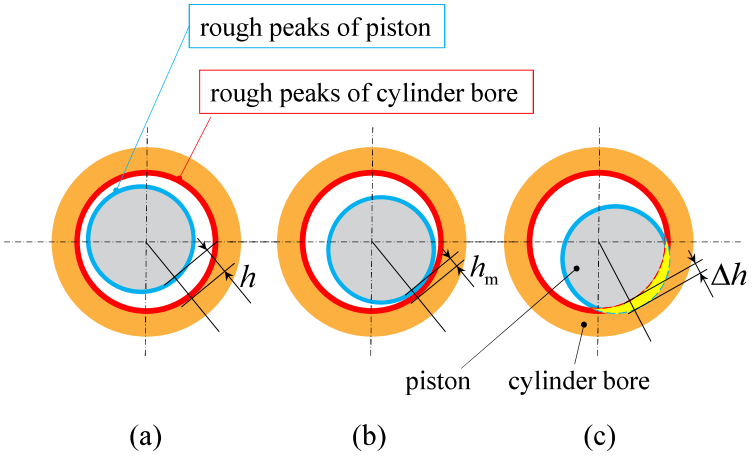

Fig. 4: Cross-section of the piston/cylinder pair in different cases

The hydrodynamic pressure of the oil film p can be represented by using Reynold Equation as shown in Eq. 6:

$$\frac{\partial}{\partial x}\left(\frac{\partial p}{\partial x}\frac{h^3}{\mu}\right)+\frac{\partial}{\partial z}\left(\frac{\partial p}{\partial z}\frac{h^3}{\mu}\right)=6\left(\omega_P\frac{D_C}{2}\frac{\partial h}{\partial x}+u\frac{\partial h}{\partial z}+2\frac{\partial h}{\partial t}\right) \tag{6}$$

where μ is the viscosity of the oil, and ω_P is the spinning speed of piston, u is the sliding velocity of the piston surface. For the stability of calculation, the oil film thickness h is regarded as h_m when the calculated result of Eq. 2 is less than h_m. In Eq. 6, the first two items on the right side of the equation represent the dynamic pressure effect of the wedge-shaped oil film pair, and the third item represents the squeezing effect of oil film caused by the micro-radial motion of the piston. It is difficult to solve Eq. 6 because it is a partial differential equation with the diffusion term and the source term. Therefore, the finite volume method is used to discretize the oil film and the Cyclic Tridiagonal Matrix Algorithm (CTDMA) is applied to solve the oil film pressure field of the piston/cylinder pair. The pressure field is divided into $a \times c$ grids and can be expanded to a plane for intuitive as shown in **Fig. 5**. In the contrast to the pressure field, the grid area of oil film thickness field is a quarter of the pressure field to avoid false diffusion.

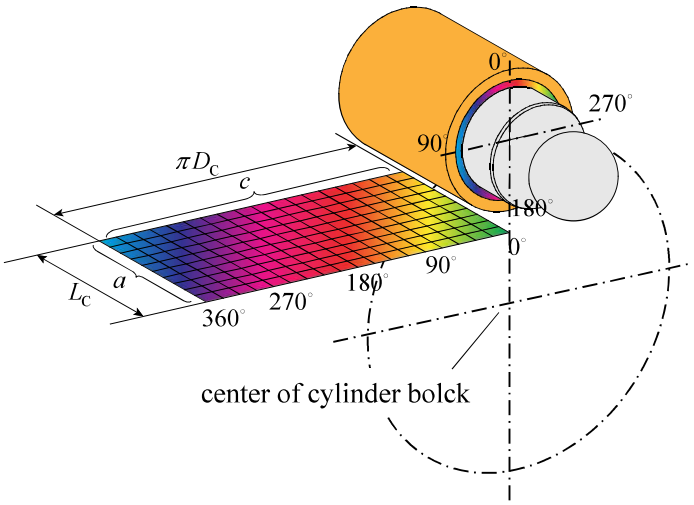

Fig. 5: Divided oil film of piston/cylinder pair

An initial oil film thickness field and corresponding thickness changing rates are assigned in Eq. 6. The pressure distribution of piston/cylinder pair oil film can be achieved by solving the discretized Reynolds Equation in order to determine the oil film reaction force on the piston. Then, the Newton-Raphson method is used for the iterative solution of the piston force balance equation. The oil film thickness and the thickness varying rate will be adjusted automatically until the deviation of force balance is less than a given threshold. Empirically, the calculated LBLPs of one revolution show cyclicity after four computing cycles, which indicates that the calculation is converged and then the calculated result of the last revolution is output.

Fig. 6 shows the calculation process of the LBLPs. In **Fig. 6**, k is the rotated angle of the cylinder with the resolution of 1 degree. The simulated results show periodicity after about 3 cycles (360 degrees per cycle) of simulation according to the experience of using this simulation model. Therefore, when the number of simulation cycles is equal to or greater than 4, the simulation is considered to converge and the results of LBLPs are output. $\Delta\dot{\boldsymbol{e}}$ is the variation of $\dot{\boldsymbol{e}}$ in each iteration, and it varies automatically using the Newton-Raphson method. F_{b} is the threshold of the force balance deviation which equals 0.1N. The Newton –Raphson method for solving nonlinear equations is completed when the converge condition $\left\|f\left(\dot{\boldsymbol{e}}_k\right)\right\| \le F_{\mathrm{b}}$ is satisfied. The wear profile of the entire cylinder bore $\boldsymbol{w}$ is obtained by using the wear calculation model introduced in the following section, and the discretized oil film thickness $\boldsymbol{h}$ is determined by wear depth $\boldsymbol{w}$ and the posture of the piston $\boldsymbol{e}$.

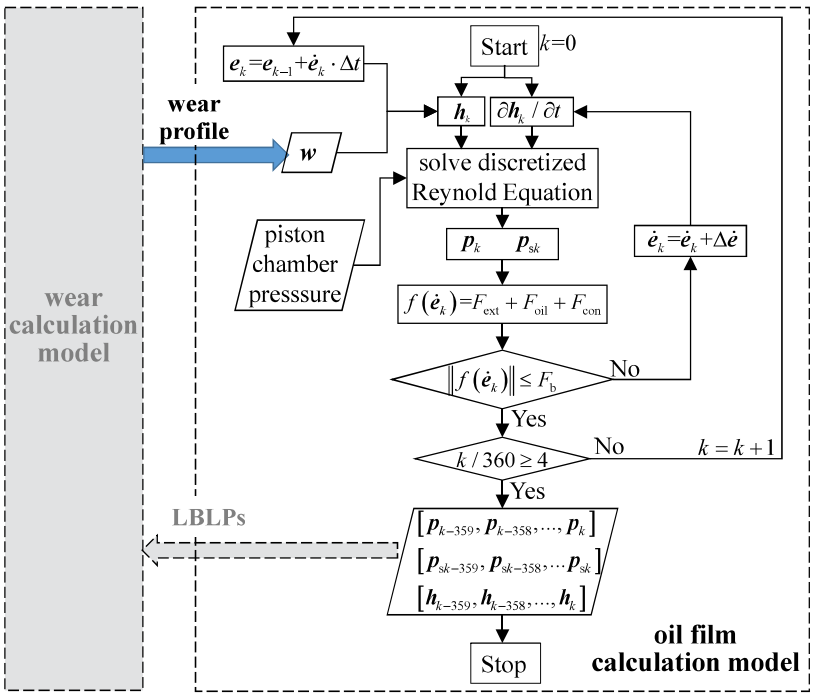

Fig. 6: Schematic diagram of LBLPs calculation

2.3. Influence of LBLPs on wear calculation

The LBLPs determine the load-bearing and lubrication conditions of the piston/cylinder pair.

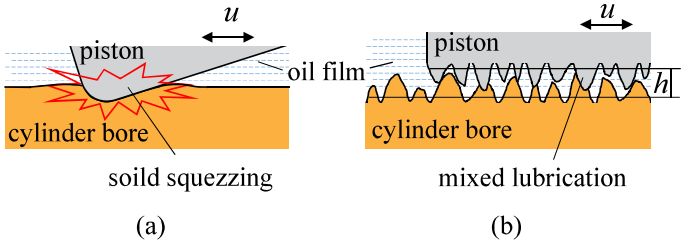

Fig. 7: Load-bearing and lubrication conditions of piston/cylinder pair

As shown in **Fig. 7**(a), the external force is too large for the oil film to provide enough reaction force to balance it. The piston and the cylinder squeeze and slide against each other. The oil film is broken when the solid contact pressure is very large. In this case, the oil film thickness h calculated by Eq. 2 can be negative. In order to represent the actual situation, the oil film thickness is considered as zero.

As shown in **Fig. 7**(b), the roughness peaks of the piston surface contact with the cylinder bore. In this case, the oil film is not broken yet, and the solid contact pressure is small. The roughness peaks of the piston are visco-elastic. When the roughness peaks slide against the cylinder bore, it could take time for them to deform. If the acting time is less than the deforming time, the roughness peaks cannot deform thoroughly, and they will run into the cylinder bore [26]. When the thickness of the oil film is thinner than h_t which represents the height of the rough peak after viscoelastic deformation, it is considered that this is a mixed lubrication condition that could give rise to sliding wear. The expression of h_t is shown in:

$$h_t = \delta_0 / e^{\Delta/2u\tau} \tag{7}$$

where δ_0 is the height of roughness peak, Δ is the wavelength of roughness peak, τ is the delay time of the piston material. The h_t is the height of the rough peak after viscoelastic deformation which is lower than the h_m. When the calculated oil film thickness is thinner than h_m, the contact of roughness peaks contributes to the load-bearing of friction pairs. However, the lubricating condition is still oil lubrication as long as the oil film thickness is larger than h_t.

The wear does not occur when the thickness of the oil film thickness is higher than h_t.

We defined the case in **Fig. 7**(a) as condition (a) and the case in **Fig. 7**(b) as condition (b), and the load-bearing and lubrication conditions can be judged as:

$$\begin{cases} h = 0 & \text{condition (a)} \\ 0 < h \le h_t & \text{condition (b)} \end{cases} \tag{8}$$

The wear mechanisms are multifarious under different load-bearing and lubrication conditions. The adhesive nodes will increase when the solid squeezing occurs as shown in **Fig. 7**(a). And the adhesive nodes may lead to shearing fracture and surface abrasion. The wear depth w can be calculated by using the adhesive wear model as shown in Eq. 9[17]:

$$\mathrm{d}w=k_{\mathrm{s}}\frac{p_{\mathrm{s}}}{3\sigma_{\mathrm{s}}}\mathrm{d}s \tag{9}$$

where s is the sliding distance, σ_{s} is the compressive yield limit which is related to the rigidity of the worn material, k_{s} is the wear coefficient which is always determined by experiments. The material of the piston is steel, and it is copper for cylinder bore in general. The worn surface is cylinder bore which is much softer than the piston, in accordance with the actual wear situation of the commercial axial piston pump.

As shown in **Fig. 7**(b), the oil film pressure is insufficient to form the adhesive nodes. However, the sliding wear will occur when the height of the roughness peak after viscoelastic deformation is higher than the oil film thickness. The wear depth of the cylinder bore can be calculated by the partial-EHL contacts sliding wear model as shown in Eq. 10[26]:

$$\mathrm{d}w=\frac{u\mathrm{d}t}{\mathrm{d}A}\left[\delta_0 e^{-\Delta/2u\tau}-h\right]^2\frac{\Delta}{\delta_0} \tag{10}$$

where t is the sliding time, and A is the wear area which is equal to the grid area of oil film thickness field. The LBLPs are the significant parameters of the wear calculation methods. As for the adhesive wear, the load on the worn surface is presented by the solid contact pressure p_{s}. For partial-EHL contacts sliding wear, the comparison of oil film thickness h and the roughness peak height is very important.

The wear calculation model is shown in **Fig. 8**. The LBLPs are discretized into each grid to judge the wear mechanism and used to calculate the wear depth. The wear depth of each grid dw is synthesized into the wear profile of the entire cylinder bore $\boldsymbol{w}$. The surface profile of the piston/cylinder pair will change after the wear occurs, which affects the calculation of LBLPs, and the LBLPs also influence the calculation of wear process.

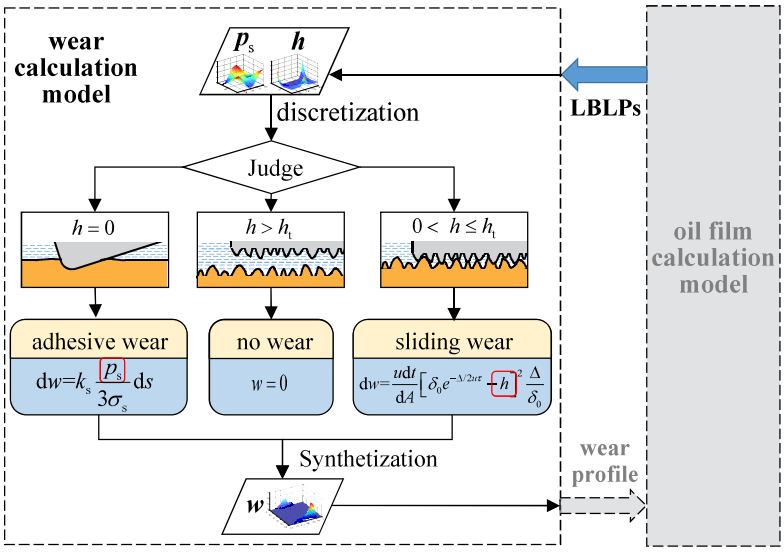

Fig. 8: Schematic diagram of the wear calculation model

2.4. Process of the wear prediction method

The interaction between the surface wear and the LBLPs has been clarified in section 2.3. However, the wear depth caused by one revolution of the pump is insufficient to impact the LBLPs and it is time-consuming to recalculate the oil film after each revolution. Therefore, a wear depth threshold w_t is set to determine whether the oil film needs to be recalculated. The wear profile of one revolution is superimposed on the previous wear until the threshold value w_t is exceeded and then the oil film is recalculated.

In the wear prediction method, the structural parameters, material parameters, working conditions and parameters in simulations are listed in **Table 1**.

Table 1 Parameters using for the wear prediction method

Parameters	Values	
Diameter of cylinder bore	28	[mm]
Length of cylinder bore	46.5	[mm]
Axial length of piston surface	64.1	[mm]
Angle of swash plate	15	[°]
Brinell hardness of cylinder bore	270	[MPa]
Elastic modulus of cylinder bore	106	[GPa]
Elastic modulus of piston	206	[GPa]
δ_0 of piston surface	0.7735	[μm]
Δ of the piston surface	35.2	[μm]
Pressure in pump shell	0.5	[MPa]
Outlet pressure	43	[MPa]
Rotational speed	1450	[rpm]
Number of pressure field grids in the circumferential direction	17	[-]
Number of pressure field grids in the axial direction	44	[-]
Force balance deviation	0.1	[N]
Number of simulation cycles of LBLPs calculation	4	[-]

The contact length of the piston and the cylinder bore vary with the rotating cylinder. The curve of the contact length and corresponding contact states is plotted based on the structure of the simulated pump. as shown in **Fig. 9**.

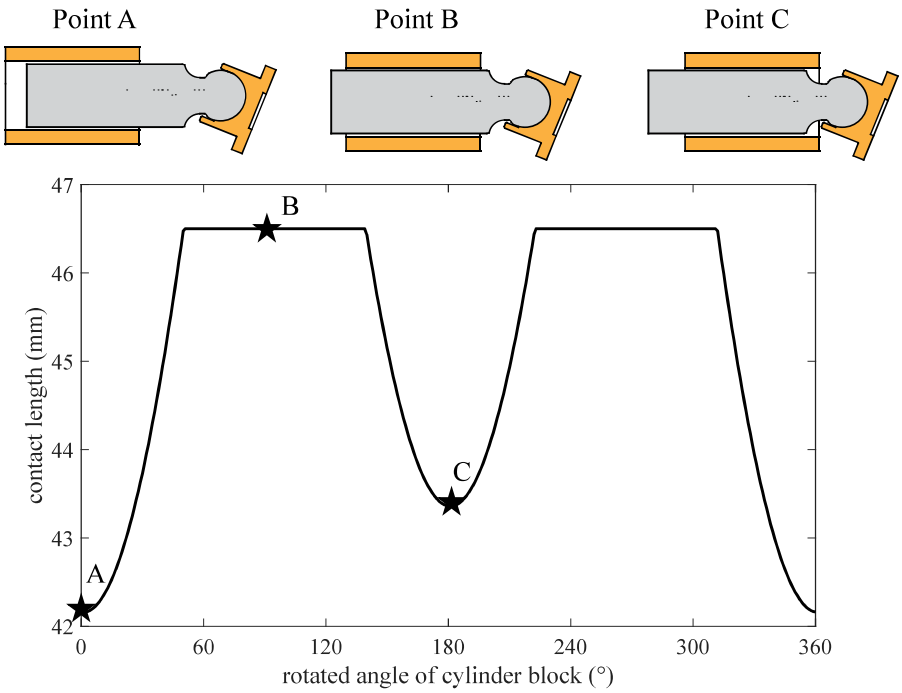

Fig. 9: Contact length of piston and cylinder bore

The pressure in the piston chamber is a crucial boundary condition that needs to be obtained by Computational Fluid Dynamics (CFD) model. It is related to the working condition of the pump like inlet and outlet pressure. and determines the pressure force F_p, as shown in **Fig. 2**. The simulation model of the axial piston pump is created based on a commercial CFD platform. The result of the piston chamber pressure is shown in **Fig. 10**.

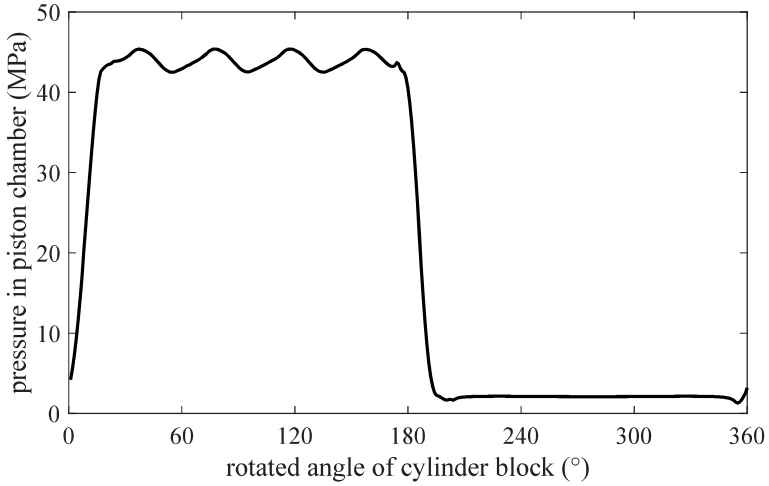

Fig. 10: Simulated result of piston chamber pressure

The time-varying wear process of the cylinder bore in certain working conditions can be obtained by the following process.

1. The LBLPs are calculated by the oil film calculation model.
2. The LBLPs are fed into the wear model as the inputs to obtain the wear profile of one revolution.
3. As described earlier in section 2.4, in order to make the calculation more efficient, the wear profile is superimposed linearly with the number of revolutions until the wear depth exceeds the threshold w_t.

4. When the threshold is exceeded, the wear profile will be input to the oil film model to recalculate the LBLPs. At the same time, the wear profile is updated as the outputs. The corresponding operating time can be calculated by the revolutions of the pump and the rotational speed ω.

5. The above steps are repeated until the total operating time T_m is reached.

The schematic diagram of the method is shown in **Fig. 11**.

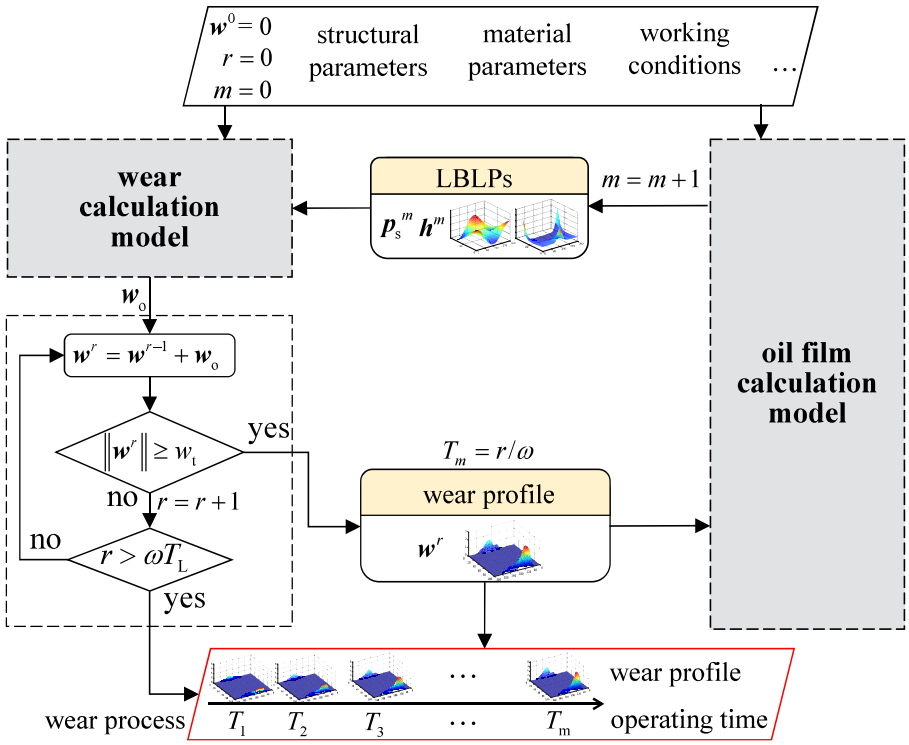

Fig. 11: Schematic diagram of the wear prediction method

In **Fig. 11**, r is the revolution of the pump, m is the count of LBLPs calculation. $\boldsymbol{w}_o$ is the wear profile of the entire cylinder bore during one revolution, $\boldsymbol{w}^r$ is the wear profile of the entire cylinder bore during r revolutions, $\boldsymbol{w}^0$ is the initial wear profile.

3. Experimental Investigation

3.1. Axial pump testing

A commercial axial pump was tested to analyze the wear regions and corresponding wear depth of the cylinder bore. The test lasted for 240 hours on an accelerated lifetime testing bench. The accelerated lifetime testing condition is consistent with the simulated conditions as listed in **Table 1**. The loading pressure of the test pump for an accelerated lifetime test is 1.23 times higher compared to the normal working pressure which is 35MPa. **Fig. 12** shows the testing bench, which was built according to the Standard JB/T7043-2006 [27].

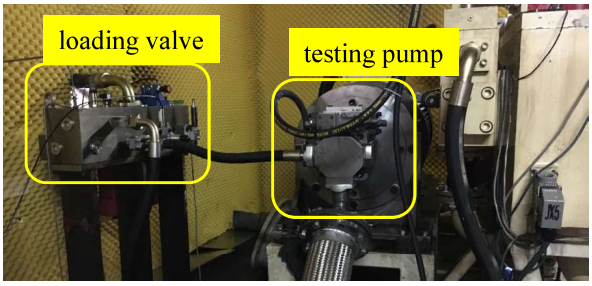

Fig. 12: Testing bench and the axial pump

3.2. Wear measurement

The pump was disassembled and the cylinder block was taken out before and after the accelerated lifetime test so that the wear of the cylinder bore could be measured. The coordinate measuring machine (CMM) is utilized to measure the circumferential profile of the cylinder bore in micron scale. The circumferential profile of the section on the cylinder bore is obtained after the CMM probe scans the inner wall of the cylinder bore. The resolution of the measuring equipment is smaller than 1μm, and it is sufficient to meet the requirement of wear measurement. **Fig. 13** shows the measurement of the cylinder bore and the sites of the measured sections.

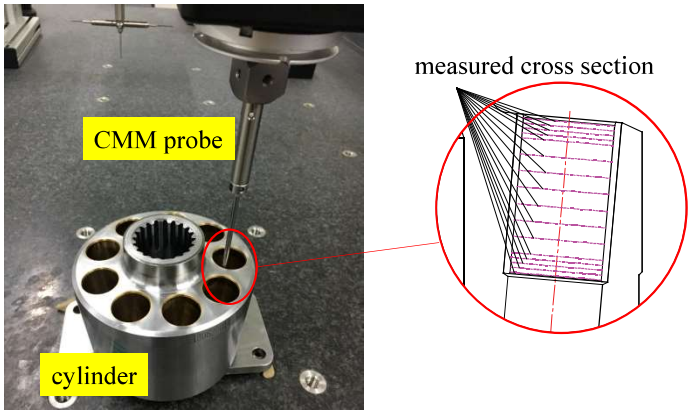

Fig. 13: Measurement of the cylinder bore

The circumferential profiles of the sections can be fitted into the three-dimensional profile of the entire cylinder bore. It can be inferred that the axial wear gradient near both ends of the cylinder is more significant than that elsewhere due to the structure of the piston/cylinder and the force condition, as shown in **Fig. 2**. This is because the measured sections near both ends of the cylinder were more intensive than that elsewhere.

The three-dimensional profiles of the cylinder bore before and after the accelerated lifetime test are shown in **Fig. 14**.

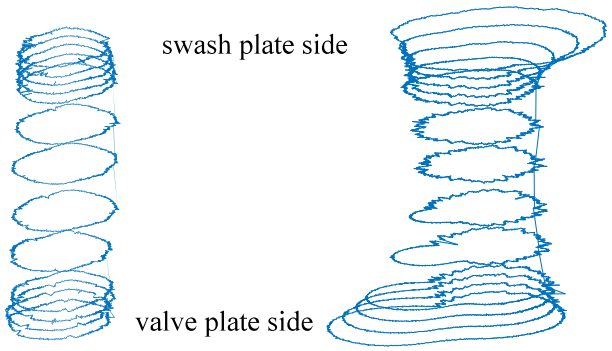

Fig. 14: Measured three-dimensional profile of the cylinder bore

The profile of the cylinder bore before the test is close to a regular cylinder and the shape and diameter of each section are almost the same, while the diameters of the sections near both ends are much larger after 240-hour test due to the wear process. The actual wear profile of the cylinder bore can be obtained by the difference of the cylinder bore profiles before and after the test. It can be expanded to a plane as shown in **Fig. 15**. It is expanded in the same way as **Fig. 5**. The vertical axis represents the wear depth w. The tested piston surface was measured using the same method, but no obvious wear profile was found.

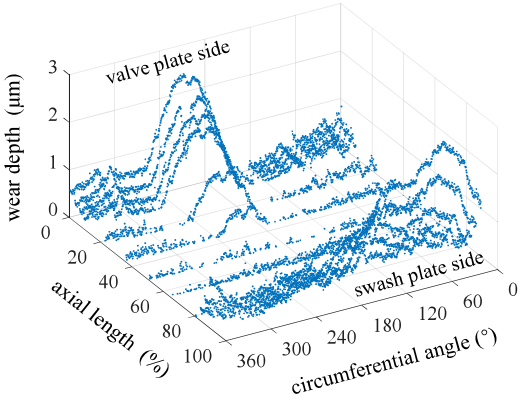

Fig. 15: Measured wear profile of the cylinder bore

4. Analysis and discussion

4.1. Determination of the wear coefficient

For the adhesive wear model mentioned in section 2.3, k_s is a crucial coefficient that represents the probability of adhesive nodes formation. However, the determination of k_s is quite difficult, because it varies with different load-bearing and lubrication conditions, and there are no theoretical criteria to choose it currently.

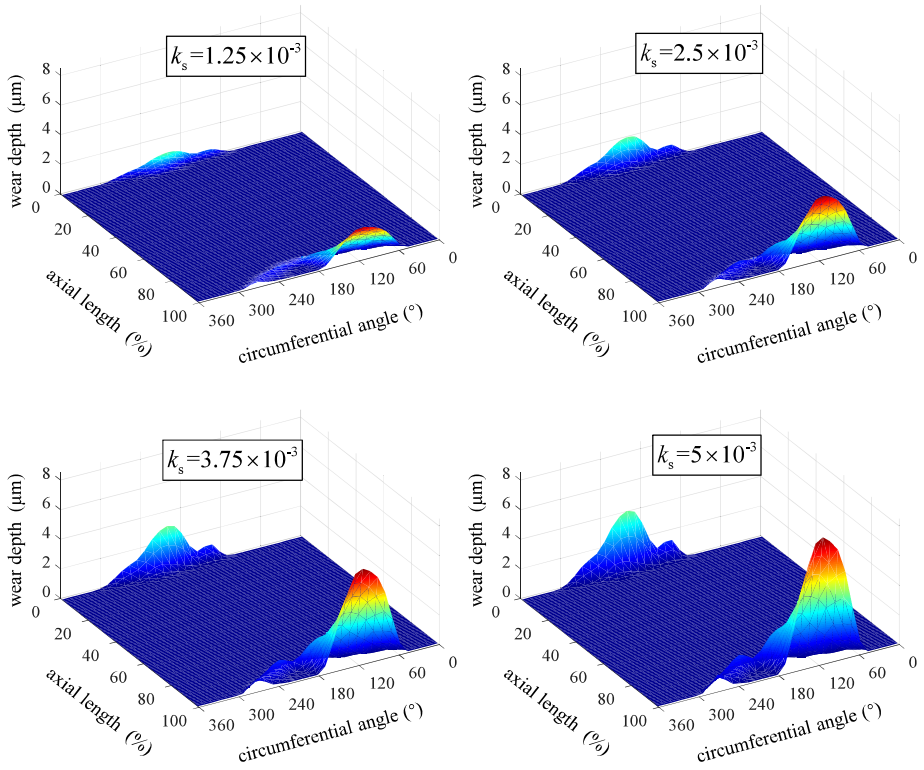

Fig. 16: Simulated results with different k_s

Fig. 16 shows four different simulated results with a variety of k_s (k_s =1.25×10^{-3}, 2.5×10^{-3}, 3.75×10^{-3} and 5×10^{-3}). The k_s has little effect on where the wear is, but it has great effects on the depth of wearing. The determination of k_s is crucial for the wear calculation.

The measured result is utilized to determine the value of k_s. The discrepancy between the simulated and the measured results represent the appropriateness of the selected value of k_s. The smaller the discrepancy is, the more appropriate the k_s value is. The residual sum of squares (RSS) is widely used to measure the degree of correlation between two variables. It can be used to quantitatively describe the discrepancy between the simulated and measured results as shown in Eq. 11:

$$RSS=\sum\left(w_m-w_s\right)^2, \tag{11}$$

where w_m is the measured wear depth, and w_s is the simulated wear depth.

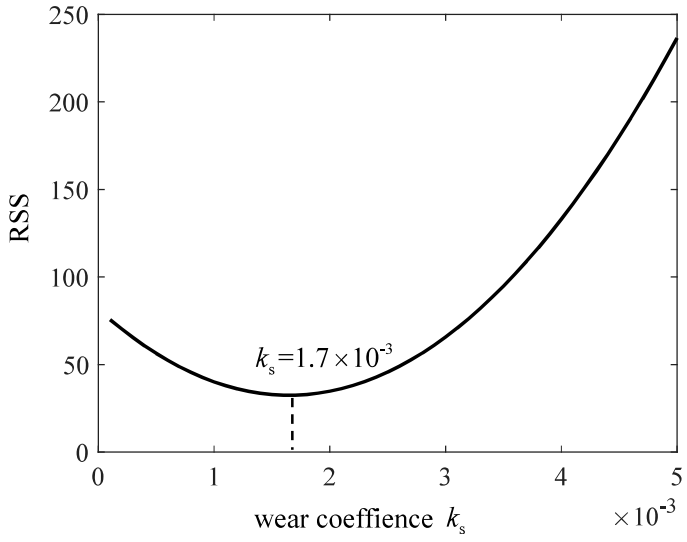

Fig. 17: Relationship between *RSS* and k_s

The relationship between RSS and k_s is shown in **Fig. 17**. The simulated result reaches the best approximation to the measured result when RSS reaches the minimum value. Therefore, the value of k_s in the simulation model is set as 1.7×10^{-3}.

4.2. Comparison between simulated and measured results

The simulated wear distribution can be obtained as shown in **Fig. 18**(a) after determining the value of the wear coefficient k_s. Both the simulated and measured results show that the most severe wear regions are near the ends of the cylinder bore. However, the circumferential angles for the two peak values are different.

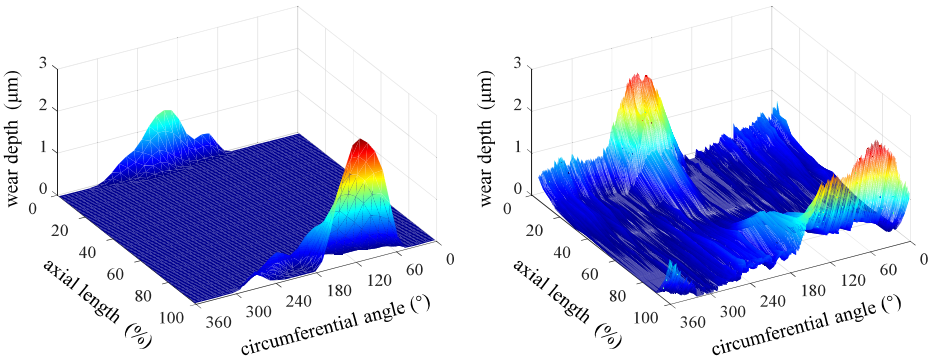

(a) simulated result (b) measured result

Fig. 18: Entire wear profile of the cylinder bore

The circumferential wear profiles at both ends of the cylinder bore are shown in **Fig. 19** for a comparison.

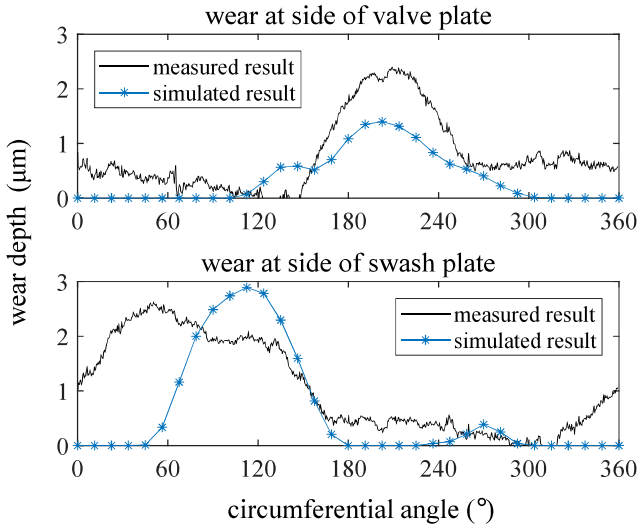

Fig. 19: Circumferential profile of the cylinder bore

The measured result shows that there is severe wear between 150° and 250° at the side of the valve plate. And the range is -50° to 180° for the side of swash plate. It can be seen that the simulated result is generally consistent with the measured result, but there are still some deviations. The simulation model of LBLPs is based on several hypotheses [28], which could cause the inevitable deviation of lubricating condition judgement between simulation and complicated actual state. There are

discrepancies between the wear models and the actual wear mechanism, for example, the neglect of abrasive wear due to the tiny metal particles in hydraulic oil. The accuracy of the proposed model is acceptable and can be used to investigate the relationship between the wear process and operating and structural parameters of piston/cylinder pairs, which can be very useful for analysing the failure mechanism and predicting the lifetime of axial pistons pumps.

4.3. Discussions

The proposed method can be used to predict the wear process of the piston/cylinder pair which is useful to pump monitoring and maintenance. **Fig. 20** shows the simulated results of the wear process of the piston/cylinder pair under an accelerated lifetime testing condition. It must be acknowledged that the wear coefficient varies with actual working conditions and operating time of axial piston pumps in practice. The predicted wear process of cylinder bore under the accelerated lifetime test condition, based on the wear coefficient in **Fig. 17**, is only suitable for this tested axial piston pump in the discussed working conditions.

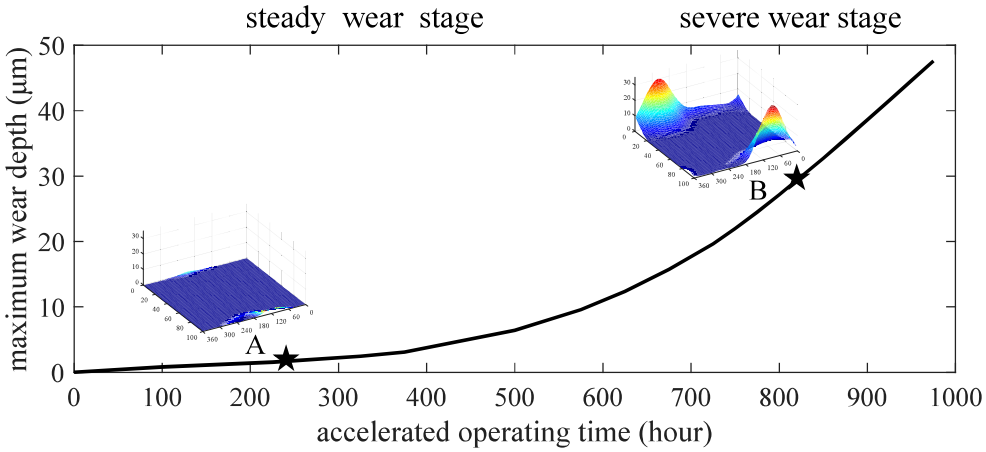

Fig. 20: Wear process of cylinder bore under accelerated lifetime testing condition

A typical sliding wear process can be explained with three characteristic stages, running-in wear, steady-state wear and accelerated wear according to the wear rate and the maximum wear depth [28]. In Fig. 20, the wear degree and wear rate both change with operating time, which is in accordance with the common wear mechanism.

For the 240-hour accelerated test of the pump in this paper, the wear condition of the piston/cylinder pair is at point A which is at the steady-state wear stage in **Fig. 20**. The point B is selected for comparison, where a rapid increase of wear rate and considerable maximum wear depth occurred, which indicates that the axial piston pump bears the risk of a sudden failure.

In addition, the axial friction and the leakage at the accelerated wear stage is worse than that at the steady-state wear stage. **Fig. 21** shows the axial friction and leakage in one revolution at point A and point B, respectively, which indicates sharp reduction of efficiency of the axial piston pump.

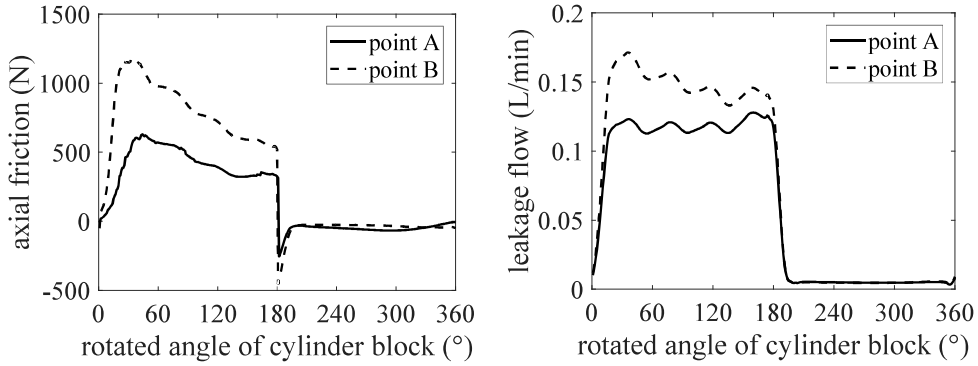

Fig. 21: Axial friction and leakage at point A and point B

5. Conclusion and outlook

A method to predict the wear process of the piston/cylinder pair was proposed in this paper. The following conclusions can be made.

(1) With a 240-hour accelerated test, the value of the wear coefficient is determined as 1.7×10^{-3}, when the discrepancy between simulated and measured results was minimized.

(2) The simulated and measured results show that the wear of two ends of the cylinder bore is severe. The severe wear occurs in the specific ranges of circumferential angle.

(3) The wear process of the piston/cylinder pair is useful to obtain the maintenance time of the axial piston pump.

The LBLPs calculation model is related to the working conditions of the piston pump, such as outlet pressure and rotational speed. These factors are used as accelerated variables in the accelerated life test. Through the study of this paper, the wear process under different accelerated conditions can be obtained, which is significant for the research about the accelerated life test for piston pumps.

Acknowledgements

The research was financially supported by the National Key Research and Development Program of China (Grant No. 2019YFB2004504), the National Natural Science Foundation of China (Grant No. 51835009) and the National Natural Science Foundation of China (Grant No. U1737110).

References

Primary Sources

Secondary Sources

Uncategorized References

[1] H.-y. Yang, M. Pan, Engineering research in fluid power: a review, Journal of Zhejiang University-Science A, 16 (2015) 427-442.
[2] N. Manring, Fluid power pumps and motors: analysis, design and control, McGraw Hill Professional, 2013.

[3] S. Xia, J. Zhang, S. Ye, B. Xu, W. Huang, J. Xiang, A Spare Support Vector Machine Based Fault Detection Strategy on Key Lubricating Interfaces of Axial Piston Pumps, IEEE Access, 7 (2019) 178177-178186.
[4] S. Gels, Einsatz konturierter und beschichteter Kolben-Buchse-Paare in Axialkolbenmaschinen in Schrägscheibenbauweise, Shaker, 2011.
[5] H. Meng, K. Ludema, Wear models and predictive equations: their form and content, Wear, 181 (1995) 443-457.
[6] H.-J. van der Kolk, Beitrag zur Bestimmung der Tragfähigkeit des stark verkanteten Gleitlagers Kolben/Zylinder an Axialkolbenpumpen der Schrägscheibenbauart, Verlag nicht ermittelbar, 1972.
[7] Y. Fang, M. Shirakashi, Mixed lubrication characteristics between the piston and cylinder in hydraulic piston pump-motor, (1995).
[8] M. IVAN TYSYNOVA, Theoretische und experimentelle Untersuchungen zu einem neuen Kolbentyp für Axialkolbenmaschinen, Schmierungstechnik, 19 (1988) 170-173.
[9] M. Ivantysnova, Temperaturfeld im schmierspalt zwischen kolben und zylinder einer axialkolbenmaschine, Maschinenbautechnik, 34 (1985) 532-535 %@ 0025-4495.
[10] L. Olems, Investigations of the temperature behaviour of the piston cylinder assembly in axial piston pumps, International Journal of Fluid Power, 1 (2000) 27-39.
[11] U. Wieczorek, M. Ivantysynova, Computer aided optimization of bearing and sealing gaps in hydrostatic machines—the simulation tool CASPAR, International Journal of Fluid Power, 3 (2002) 7-20.
[12] A. Fatemi, A. Wohlers, H. Murrenhoff, Simulation of elastohydrodynamic contact between piston and cylinder in axial piston pumps, Proc. of the 6th International Fluid Power Conference, 2008, pp. 539-552.
[13] G. Sanchen, Simulationswerkzeug zur Auslegung von Axialkolbenpumpen in Schragscheibenbauweise, O+ P. Ölhydraulik und Pneumatik, 43 (1999).
[14] G. Sanchen, Auslegung von Axialkolbenpumpen in Schrägscheibenbauweise mit Hilfe der numerischen Simulation, Shaker, 2003.
[15] S. Gels, H. Murrenhoff, Simulation of the lubricating film between contoured piston and cylinder, International Journal of Fluid Power, 11 (2010) 15-24.
[16] B. Xu, J. Zhang, H. Yang, B. Zhang, Investigation on the radial micro-motion about piston of axial piston pump, Chinese Journal of Mechanical Engineering, 26 (2013) 325-333.
[17] J. Archard, Contact and rubbing of flat surfaces', Journal of Applied Physics, vol, 24 (1953) 918-988.
[18] G. Fleischer, Energy Balance in the Friction of a Solid Body as the Basis of Energetic Wear Calculations, Schmierungstechnik, 7 (1976) 271-275.
[19] S. Wu, H. Cheng, A sliding wear model for partial-EHL contacts, (1991).
[20] L. Ting, J. Mayer Jr, Piston ring lubrication and cylinder bore wear analysis, part I—theory, (1974).
[21] P. Nautiyal, S. Singhal, J. Sharma, Friction and wear processes in piston rings, Tribology International, 16 (1983) 43-49.
[22] D. Bartel, L. Bobach, T. Illner, L. Deters, Simulating transient wear characteristics of journal bearings subjected to mixed friction, Proceedings of the Institution of Mechanical Engineers, Part J: Journal of Engineering Tribology, 226 (2012) 1095-1108.
[23] J. Ma, J. Chen, J. Li, Q. Li, C. Ren, Wear analysis of swash plate/slipper pair of axis piston hydraulic pump, Tribology International, 90 (2015) 467-472.
[24] S. Wen, P. Huang, Principles of tribology, Wiley Online Library, 2012.
[25] E.J. Hearn, Mechanics of Materials 2: The mechanics of elastic and plastic deformation of solids and structural materials, Elsevier, 1997.
[26] Q. Zou, P. Huang, Abrasive wear model for lubricated sliding contacts, Wear, 196 (1996) 72-76.
[27] Hydraulic Axial Piston Pumps, Mechanical Industry Press, Beijing, 2006.
[28] A.M. Wondergem, M. Ivantysynova, The impact of micro-surface shaping on the piston/cylinder interface of swash plate type machines, ASME/BATH 2015 Symposium on Fluid Power and Motion Control, American Society of Mechanical Engineers Digital Collection, 2015.